Supporting Information

UV photostability of three 2-aminoazoles with key roles in prebiotic chemistry on the early Earth

Zoe R. Todd, Rafal Szabla, Jack W. Szostak, Dimitar D. Sasselov

Table of Contents

1. General Methods

2-aminooxazole (97%) and 2-aminoimidazole hemisulfate (98%) were purchased from CombiBlocks. 2-aminothiazole (97%) was purchased from Sigma Aldrich. For irradiation experiments, a 0.1 mM solution of the molecule of interest was prepared in deionized water. The sample was transferred to a Spectrosil quartz cuvette with a screw top (Starna Cells part number 9-Q-10-GL14-C) and a micro-stirbar was added. Before irradiation, an initial UV-Vis absorption spectrum (200-350 nm) was taken using an Amersham Sciences Ultrospec 3100 pro. The sample was then irradiated in the tunable lamp setup, with irradiation wavelengths from 215-285 nm in 10 nm intervals, with a 10 nm bandwidth. The sample was continuously stirred. At periodic intervals, the sample was briefly removed from the lamp to record the UV-Vis absorption spectrum. For the more stable molecules at less destructive wavelengths, typical time points were taken every 30 minutes. For the most unstable wavelengths and molecules, time points were around 10 minutes. The duration of irradiation lasted from 1-8 hours, depending on the overall rate of the degradation.

The tunable irradiation setup (Figure S1) uses a 75W Xenon Tunable PowerArc lamp made by Optical Building Blocks (OBB). The xenon lamp coupled with a diffraction grating (acting as a monochromator) allows for tunable wavelength selection over the UV mid-range (roughly 200-300 nm). In order to allow tunable wavelength selection, the relative position of the grating with respect to the exit slit is adjusted. The sample-containing cuvette is placed on a mount with stirring capability. Irradiation experiments used a bandwidth of 10 nm, though the bandwidth is also adjustable in the setup.

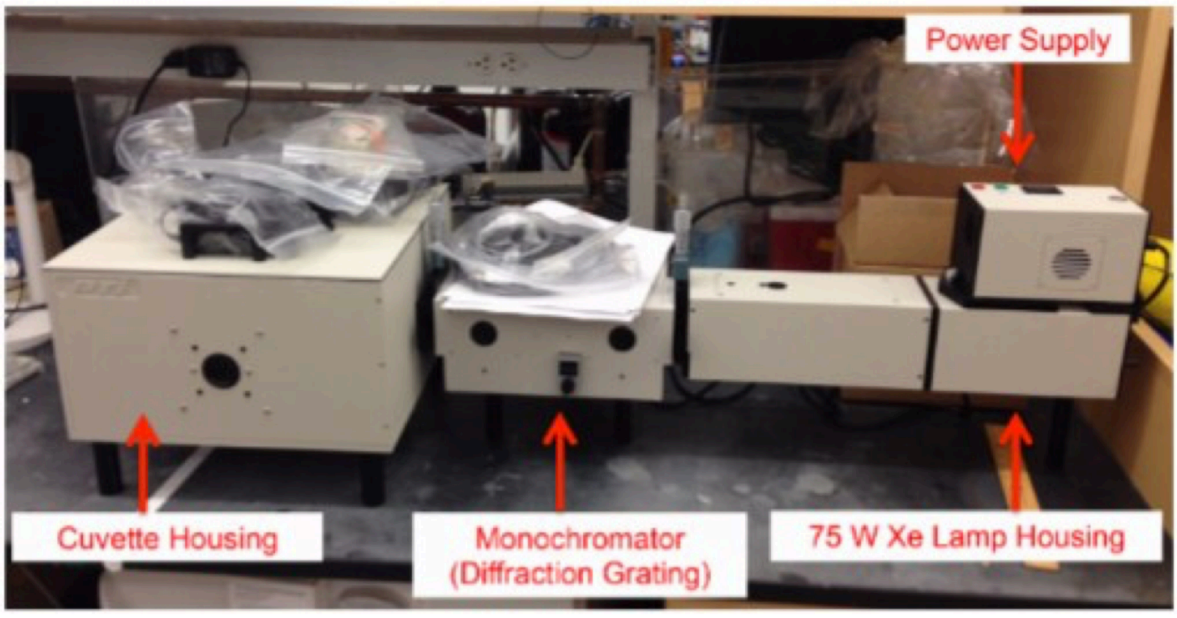

Figure S1: Optical Building Blocks 75W Tunable PowerArc lamp used for tunable wavelength irradiation experiments. A xenon arc lamp is coupled with a diffraction grating to split light into separate wavelengths. Tunable wavelength selection is achieved by adjusting the position of the grating with respect to the exit slit.

2. Standard Curves

In order to convert the observed absorption spectra to concentration throughout the course of an irradiation experiment, we compiled standard curves relating absorbance to concentration for the three molecules (Figure S2). The maximum absorbance for AO, AI, and AT occurred at wavelengths of 207, 215, and 254 nm, respectively. Figure S3 shows the absorbance (at the maximum) as a function of concentration for each molecule. The equations relating these absorption values to concentrations of each molecule are:

$$conc_{AI} = 0.120A_{AI,207nm} - 0.0175$$
$$conc_{AO} = 0.153A_{AO,215nm} - 0.0162$$
$$conc_{AT} = 0.211A_{AT,254nm} - 0.0165$$

From these relations, the measured absorption values can be converted into a concentration of the given molecule throughout an irradiation experiment.

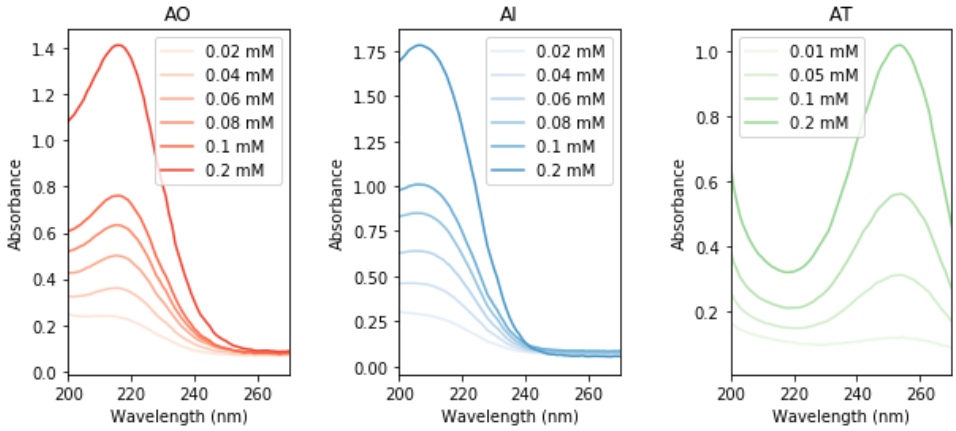

Figure S2: Standard curves for AO, AI, and AT, used to relate measured absorbances to a concentration.

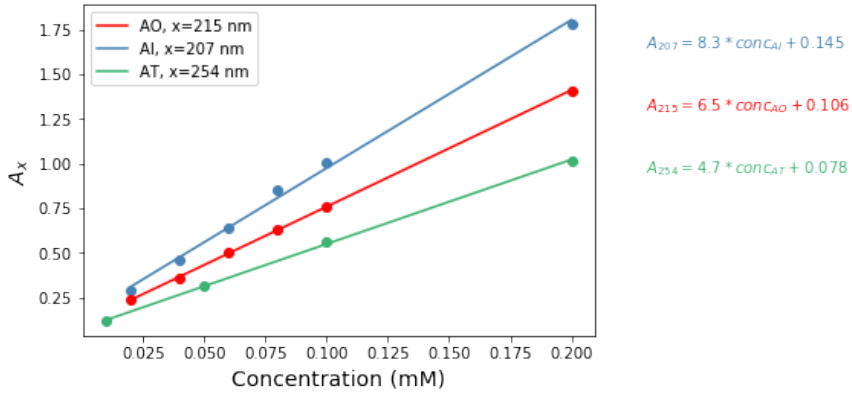

Figure S3: Absorption at the maximum wavelength for each molecule as a function of concentration. These relations can be used to calculate the concentration from measured absorption values.

3. Irradiation experiments analysis

During irradiation experiments, we monitored the photodestruction reaction by UV-Vis absorption using an Amersham Science Ultrospec 3100 Pro. Irradiations were carried out for durations of 1-8 hours, with variable timepoints depending on the total length of the experiment (see section 6). We then used the standard curves from section 2 to convert the absorbance at the absorption maximum for each molecule into a corresponding concentration. The destruction rate constant was determined by plotting ln(concentration) as a function of irradiation time, which gave a linear trend. The slope of the linear trend line gives the rate constant for the destruction reaction, and was calculated from a python fitting routine. Each irradiation wavelength for all molecules was analyzed the same way. Additionally, all irradiation wavelengths and molecules were repeated in duplicate over the range of 215-285 nm, in 10 nm intervals with 10 nm bandwidths. The duplicate wavelength rates were averaged to obtain the estimated rate, and errors were estimated from the standard deviation of the duplicate pair. However, the tunable xenon lamp emits different powers at various irradiation wavelengths, so these rates cannot yet be compared as a function of irradiation wavelength.

In order to allow for irradiation wavelength comparison, we determined the incident photon flux as a function of irradiation wavelength. To do this, the power from the apparatus was measured with a Newport power meter during each experiment. The photon flux could then be calculated by dividing the incident power by the energy of a photon at that specific irradiation wavelength (through the relation $E = hc/\lambda$).

To then compare reaction rates as a function of irradiation wavelength, we took the raw reaction rates determined from the linear plot of ln(concentration) vs. time, and normalized by the incident photon flux. These photon flux-normalized rates were then multiplied by a constant photon flux of 2.5×10^{14} phot/s to generate the normalized reaction rate (Fig 4). This photon flux is the expected solar photon flux from 210-290 nm on the surface of the early Earth (see SI section 6), which is also consistent with the typical experimental photon flux.

4. Irradiation experiments concentration dependence

We next analyzed the concentration dependence of irradiation experiments in order to determine the order of the reaction. For each molecule, we irradiated 0.05, 0.1, and 0.2 mM solutions in a Rayonet RPR-200 (254 nm) reactor for 10 minutes and monitored the reaction by UV-Vis spectroscopy. The rate constant for each reaction was determined as described above. Figure S4 shows the rate constant as a function of concentration for each molecule. We find a linear trend between rate and concentration, suggesting that the irradiation reactions are first order.

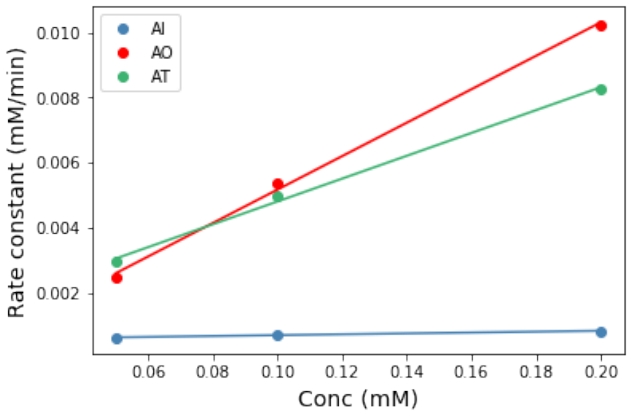

Figure S4: Concentration dependence of the photo destruction rate of each molecule. The linear trend between rate constant and concentration is indicative of first order kinetics.

5. Reaction of AO and glyceraldehyde

We attempted to compare the rate at which AO reacts on the pathway to nucleotides in a prebiotic context to the photodestruction rate, in order to determine if the presence of UV light in such a prebiotic chemical network is self-consistent. Powner et al. (2009) showed that AO can react with glyceraldehyde to form pentose aminooxazolines. The arabinose aminooxazoline undergoes further reaction to eventually yield activated pyrimidine ribonucleotides. Under the Powner et al. (2009) reaction conditions, AO is formed from reaction of glycolaldehyde (1M) and cyanamide (1M) in 1.0M phosphate (pH 7), in 3 hours as 60°C. 1M *rac*-glyceraldehyde was added, and the reaction was heated at 40°C for another 16 hours. Powner et al. (2009) found an overall 70% conversion to products including AO, arabinose aminooxazoline, ribose aminooxazoline, and other pentose aminooxazolines (xylose aminooxazoline, lyxofuranose aminooxazoline, lyxopyranose aminooxazoline), and pentose oxazoles (rac-[3R,4R]-pentose oxazole and rac-[3S,4R]-pentose oxazole).

We sought to determine the rate of the reaction of AO and glyceraldehyde at lower concentrations, so as to better compare to our experimental photodegradation timescales. We allowed unbuffered solutions of equal concentrations of AO and glyceraldehyde in D_2O to react at 40°C and monitored the reaction progress by ^{1}H-NMR. We tested concentrations of 10 mM AO + 10 mM glyceraldehyde, 1 mM AO + 1 mM glyceraldehyde, and 0.1 mM AO + 0.1 mM glyceraldehyde. The 10 mM and 1 mM experiments were heated for 16 hours, while the 0.1 mM experiment was heated for 200 hours. An aliquot of the initial sample was saved, then spiked with an internal standard, and monitored by NMR. After heating, samples were spiked with the internal standard to allow for quantitative comparison to the initial sample. We integrated the aromatic protons of AO (6.63 and 7.16 ppm) with respect to the internal standard to get a quantitative measure of the progress of the reaction (see figure S5). The internal standards were used to obtain the concentration of the aromatic protons of AO (7.16 and 6.63 ppm) at both the initial and final timepoints, as shown in Table 1.

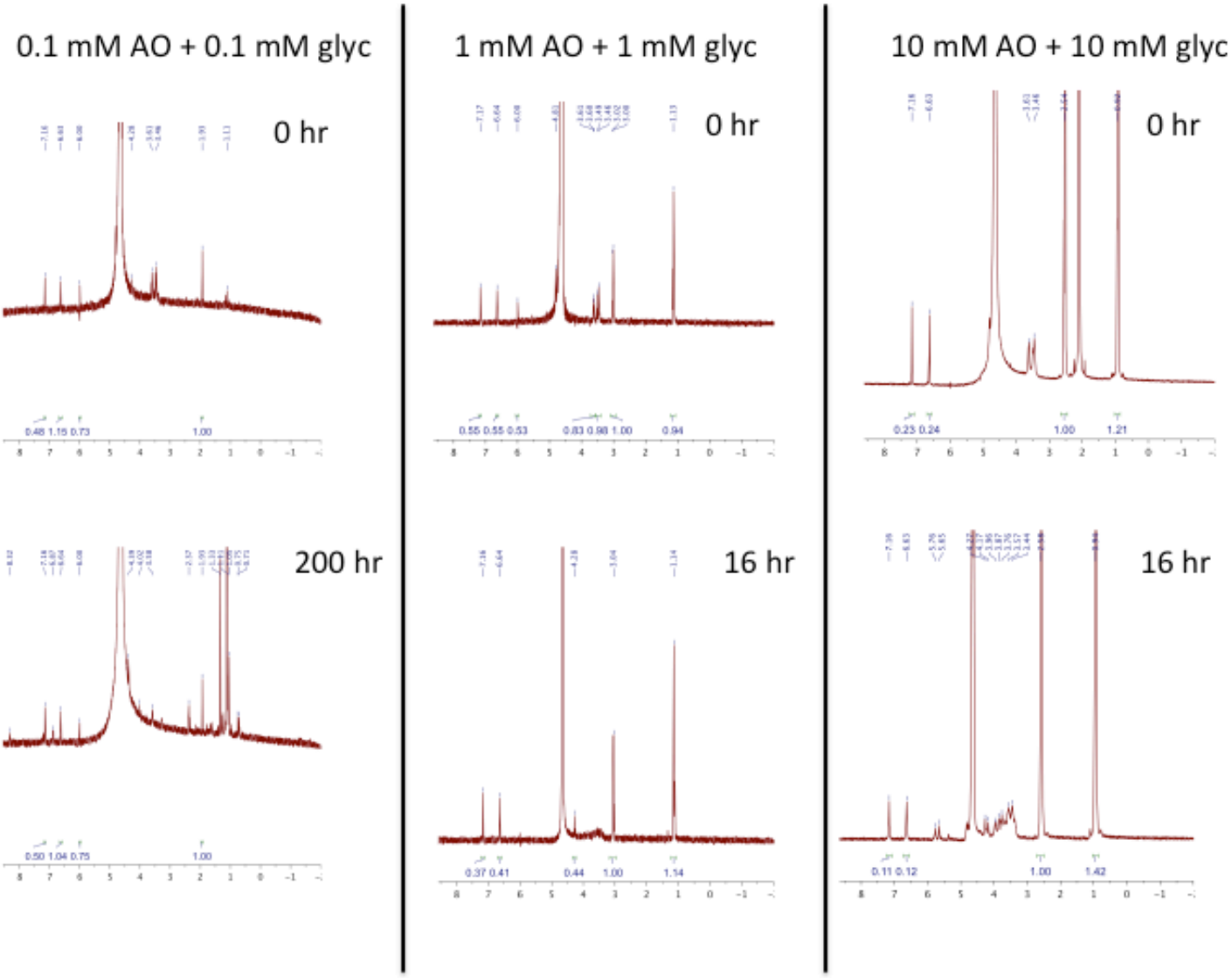

Figure S5: NMR spectra for initial and final timepoints for experiments of 0.1 mM, 1 mM, and 10 mM each of AO and glyceraldehyde. TEA was used as an internal standard in the 1 and 10 mM experiments, while acetonitrile was used for the 0.1 mM experiment. Integrating the initial and final aromatic AO proton signals (7.16 and 6.63 ppm) against the internal standard allowed for quantitative analysis of the reaction rates.

Table 1: Reaction of AO and glyceraldehyde at various concentrations. An internal standard was used to integrate the aromatic AO proton peaks at 7.16 and 6.63 ppm and allow for calculation of the concentration. With concentrations determined, we could then calculate a rate of the reaction.

10 mM AO + 10 mM glyceraldehyde				
	7.16 ppm		**6.63 ppm**	
Time (hr)	**Integral**	**Conc (mM)**	**Integral**	**Conc (mM)**
0	0.23	13.8	0.24	14.4
16	0.11	6.6	0.12	7.2
1 mM AO + 1 mM glyceraldehyde				
	7.16 ppm		**6.63 ppm**	
Time (hr)	**Integral**	**Conc (mM)**	**Integral**	**Conc (mM)**
0	0.55	1.65	0.55	1.65
16	0.37	1.11	0.41	1.23
0.1 mM AO + 0.1 mM glyceraldehyde				
	7.16 ppm		**6.63 ppm**	
Time (hr)	**Integral**	**Conc (mM)**	**Integral**	**Conc (mM)**
0	0.48	0.072	1.15	0.173
200	0.50	0.075	1.04	0.156

From the change in concentration with time, we could determine the rate of the reaction for each concentration. The average rate was determined from the rates determined from the 7.16 and 6.63 ppm signals, with the exception of the 0.1 mM experiment. In this case, only the 6.63 ppm signal gave a decreasing concentration with time, so we adopted the rate from this signal as the overall reaction rate, and only use this as an upper limit to the rate.

If we then assume that the reaction is first order in both AO and glyceraldehyde (so second order overall), the rate law can be written as:

$rate = k[AO][glyc]$

From the rate, we can determine the half life for the reaction at each concentration (table 2). At the highest concentration of 10 mM reactants, the half life is 22 hours. At 1 mM, the half-life increases to 33 hr, while the lowest concentration (0.1 mM) has a half-life >1200 hr. These are the rough timescales on which we might expect AO and glyceraldehyde to react to form the aminooxazolines that come next in the pathway, though this is by no means a complete exploration of parameter space.

Table 2: Rates and half-lives for the reaction of AO and glyceraldehyde at different concentrations. AO and glyceraldehyde are used in equal concentrations in each experiment.

Conc (mM)	**Rate (mM/hr)**	**$t_{1/2}$ (hr)**
0.1	-8.3×10^{-5}	>1200
1	-0.030	33
10	-0.45	22

Due to our experimental irradiation setup, we performed irradiations at 0.1 mM concentrations. At higher concentrations, the optical depth of the solution becomes smaller, leading to less penetration of photons which can slow the reaction. Comparing the estimated 6.9 hour half-life of 0.1 mM AO photodegradation to the reaction timescale of 0.1 mM AO + 0.1 mM glyceraldehyde (>1200 hr) does indeed make the usefulness of AO in this prebiotic scheme somewhat bleak. However, we note that the AO + glyceraldehyde reaction proceeds on the order of tens of hours at higher concentrations. At elevated concentrations, the UV degradation of AO could be lower, as the optical depth of the solution increases and could thus provide for some self-shielding. So, even though we find that AO is the most susceptible to UV damage, this may not be an insurmountable roadblock toward this prebiotic pathway. Instead, more consideration will have to be placed on the relevant concentrations possible from synthesis, and the potential for UV-shielding mechanisms.

6. Stability of AI vs. other imidazoles

Though these three molecules potentially play important roles in prebiotic chemistry, they are not the only 2-aminoazole molecules in existence. We sought to compare the photostability of three various imidazoles as a test case to understand how these prebiotic molecules compare to non-prebiotic counterparts. We irradiated 0.1 mM solutions of 2-methylimidazole, 2-ethylimidazole, and 2-aminoimidazole at 254 nm in a Rayonet reactor for 30 minutes. Rate constants were determined from the plot of ln(conc) vs. time (Figure S6), as described previously. We find that AI is considerably less photostable (rate constant of 1.05×10^{-2} min^{-1}) under these conditions that both 2-methylimidazole and 2-ethylimidazole (rate constants of 1.73×10^{-3} and 1.88×10^{-3} min^{-1}, respectively). It is interesting that the potentially prebiotically relevant 2-aminoazoles are less photostable than non-prebiotic counterparts studied here. A more complete investigation of photostabilites of various related molecules could be useful for further understanding of why these molecules may or may not be relevant and under what environments and circumstances they could be used.

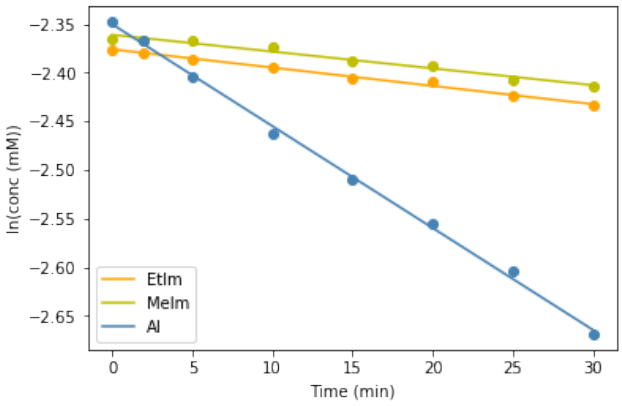

Figure S6: Irradiations of 2-methylimidazole (MeIm) and 2-ethylimidazole (EtIm) compared to 2-aminoimidazole at 254 nm in a Rayonet reactor. The slope of the fits of the logarithm of concentration vs. time give the rate constants for MeIm and EtIm of 1.73×10^{-3} and 1.88×10^{-3} min^{-1}, respectively, compared to 1.05×10^{-2} min^{-1} for AI. AI is therefore less photostable than the other two imidazoles tested under these select irradiation conditions.

7. Co-irradiation of AI and AO

Given the finding that AI is considerably more photostable than AO and the divergent synthesis and reactions of AO and AI, it becomes pertinent to ask if the simultaneous irradiation of the two compounds could allow for increased tolerance of AO to UV light. AI and AO can be synthesized simultaneously and have different reactivities towards glyceraldehyde, leading to a potential environment where both co-exist as they are being used for prebiotic reactions. To investigate this, we irradiated solutions of 0.1 mM AO + 0.1 mM AI and compared this to the individual irradiations. We tested this reaction in the Rayonet reactor (254 nm) and in the tunable setup at 215 nm. Figure S7 shows the logarithm of the maximum absorption of each solution as a function of time in the Rayonet reactor. AO and AI have very similar UV spectra, making it difficult to disentangle the two through UV-Vis measurements. For this reason, we use the absorption values at peaks wavelengths (207, 215, and 210 nm for AI, AO, and AI+AO, respectively) and note that rate constants are not precisely constrained.

In the Rayonet reactor, AO and AI have pseudo-rates of 8.1×10^{-2} and 8.6×10^{-3} min^{-1}, respectively. The combination of 0.1mM AO + 0.1mM AI has a pseudo-rate of 2.8×10^{-2} min^{-1} and 0.05mM AO + 0.05mM AI has a similar pseudo-rate of 2.9×10^{-2} min^{-1}. AO degrades the fastest, and AI the slowest, while the mixture has an intermediate destruction rate.

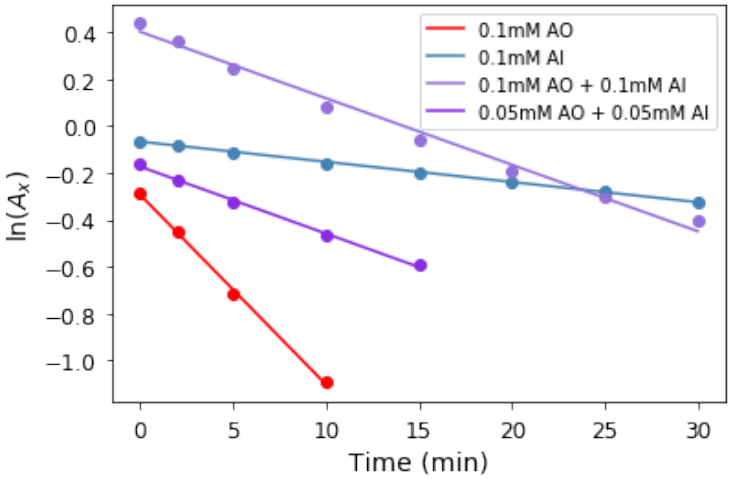

Figure S7: Logarithm of the absorbance at the peak wavelength (207, 215, and 210 nm) for solutions of AI, AO, and AO+AI with irradiation time in the Rayonet reactor. Pseudo-rates are calculated from the slopes (precise rates are difficult to determine for the AO+AI mixture due to the similar UV-Vis spectra of these two molecules). The mixtures of AO+AI have photodestruction rates in between those of AO and AI, indicating a partial protection of AO when co-irradiated with a more UV-photostable molecule, such as AI.

We also irradiated mixtures of AO and AI (0.1mM each and 0.05mM each) in the tunable setup at 215 nm (see Figure 3 of the main text). Again, given the very similar UV-Vis spectra of the two molecules, it is difficult to determine the concentration of each molecule throughout the irradiation. We instead calculated the concentrations assuming the absorption was due completely to AI and then completely due to AO. We took the average of these concentrations as a rough esti-

mate, but show the ranges in potential net concentrations ([AO]+[AI]) with the error bars in Figure 3. At 215 nm irradiation, the relative rate of photodestruction of AO and AI alone are 3.13×10^{-2} min^{-1} and 2.84×10^{-3} min^{-1}, respectively. The mixture of 0.1mM AO + 0.1mM AI has an approximate rate of 9.0×10^{-3} min^{-1}, and the 0.05mM AO + 0.05mM AI solution has an approximate rate of 1.5×10^{-2} min^{-1} (see purple points on Figure 4). Mixtures of the two molecules show degradation rates slower than that of AO alone, suggesting some potential protection of AO when co-irradiated with AI. This observation is intriguing and suggests a potential possibility for mitigating the comparatively fast photodegradation of AO simply by invoking the presence of other more UV-stable molecules. More follow-up studies along these lines could provide more stringent constraints and understanding of the potential prebiotic environment, but this is beyond the scope of this paper.

8. Atmospheric Modeling

We calculated the relative rate of the reaction on the surface of the early Earth by taking the product of the experimentally determined reaction rates and the weighted surface intensity in each wavelength bin. To calculate the weighted surface intensity, we used the code described in Ranjan and Sasselov (2017). We provide an atmospheric profile containing composition, temperature, and pressure to the code, which then calculates spectral quantities like total surface flux and total surface intensity through a two-stream clear-sky radiative transfer model. We selected two atmospheres here: one for a sample prebiotic N_2/CO_2-dominated atmosphere, and another for the modern Earth (Rugheimer et al. 2015). The exact chemical compositions of the atmospheres are listed in table 3. For the modern Earth, almost no light reaches the surface of the Earth from 200-300 nm, so we do not show the zero results. The total surface intensity through a prebiotic atmosphere was integrated in the same 10 nm intervals as experiments were carried out. These integrated surface intensities were then multiplied by the corresponding experimentally-determined photon flux-normalized reaction rate to generate the relative rate of the reaction on the surface of the planet as a function of irradiation wavelength. We then integrated these relative rates over irradiation wavelengths from 210-290 nm to estimate the total reaction rate expected on the surface of the early Earth, for a sample prebiotic atmosphere. This total rate could then be used to calculate the half life for each molecule under solar irradiation on the surface of a planet.

Table 3: Atmospheric compositions for a sample prebiotic atmosphere and the modern Eath, used for calculating the surface intensity of solar light on the planet.

	Sample Prebiotic Earth	**Modern Earth**
N_2	88.9%	78%
CO_2	10%	3.6×10^{-2}%
H_2O	0.48%	0.31%
CH_4	1.7×10^{-4}%	1.7×10^{-4}%
SO_2	3.4×10^{-9}%	0%
O_2	2.7×10^{-4}%	21%
O_3	9.2×10^{-9}%	2.4×10^{-5}%
H_2S	0%	0%

9. Tables of Experimental Values

The numerical values and associated errors for experimental data and analysis are presented in the tables below.

Table 4: Experimental parameters and results for AO experiments. The normalized rates are the experimental rates normalized by incident photon flux, and then adjusted to a constant photon flux of 2.5×10^{14} phot/s, corresponding to the photon flux expected on the early Earth.

Wavelength (nm)	**Rate1** (min^{-1})**	**t1 (min)**	**Rate2** (min^{-1})**	**t2 (min)**	**Avg. Rate (min^{-1})**
215	2.9×10^{-2}	60	3.4×10^{-2}	60	$(3.1 \pm 0.2) \times 10^{-2}$
225	2.5×10^{-2}	60	2.7×10^{-2}	60	$(2.6 \pm 0.1) \times 10^{-2}$
235	1.2×10^{-2}	75	1.3×10^{-2}	70	$(1.3 \pm 0.01) \times 10^{-2}$
245	3.6×10^{-3}	120	3.8×10^{-3}	90	$(3.7 \pm 0.1) \times 10^{-3}$
255	7.4×10^{-4}	180	9.0×10^{-4}	150	$(8.2 \pm 0.8) \times 10^{-4}$
265	3.8×10^{-4}	180	4.1×10^{-4}	180	$(4.0 \pm 0.1) \times 10^{-4}$
275	2.1×10^{-4}	180	3.0×10^{-4}	180	$(2.6 \pm 0.4) \times 10^{-4}$
285	1.7×10^{-4}	180	1.9×10^{-4}	180	$(1.8 \pm 0.1) \times 10^{-4}$

Table 5: Experimental parameters and results for AI experiments. The normalized rates are the experimental rates normalized by incident photon flux, and then adjusted to a constant photon flux of 2.5×10^{14} phot/s, corresponding to the photon flux expected on the early Earth.

Wavelength (nm)	**Rate1** (min^{-1})**	**t1 (min)**	**Rate2** (min^{-1})**	**t2 (min)**	**Avg. Rate (min^{-1})**
215	2.9×10^{-3}	265	2.8×10^{-3}	75	$(2.8 \pm 0.07) \times 10^{-3}$
225	1.2×10^{-3}	255	1.4×10^{-3}	120	$(1.3 \pm 0.1) \times 10^{-3}$
235	4.4×10^{-4}	360	4.3×10^{-4}	210	$(4.4 \pm 0.08) \times 10^{-4}$
245	1.4×10^{-4}	330	1.0×10^{-4}	360	$(1.2 \pm 0.2) \times 10^{-4}$
255	9.7×10^{-5}	360	1.1×10^{-4}	330	$(1.0 \pm 0.06) \times 10^{-4}$
265	6.5×10^{-5}	420	4.1×10^{-5}	360	$(5.3 \pm 1.2) \times 10^{-5}$
275	3.4×10^{-5}	390	5.0×10^{-5}	360	$(4.2 \pm 0.8) \times 10^{-5}$
285	3.1×10^{-5}	480	2.7×10^{-5}	420	$(2.9 \pm 0.2) \times 10^{-5}$

Table 6: Experimental parameters and results for AT experiments. The normalized rates** are the experimental rates normalized by incident photon flux, and then adjusted to a constant photon flux of 2.5×10^{14} phot/s, corresponding to the photon flux expected on the early Earth.

Wavelength (nm)	**Rate1** (min^{-1})**	**t1 (min)**	**Rate2** (min^{-1})**	**t2 (min)**	**Avg. Rate (min^{-1})**
215	1.6×10^{-3}	180	1.5×10^{-3}	180	$(1.6 \pm 0.03) \times 10^{-3}$
225	1.4×10^{-3}	180	1.6×10^{-3}	150	$(1.5 \pm 0.08) \times 10^{-3}$
235	1.6×10^{-3}	90	1.3×10^{-3}	180	$(1.4 \pm 0.1) \times 10^{-3}$
245	1.8×10^{-3}	90	1.3×10^{-3}	180	$(1.6 \pm 0.3) \times 10^{-3}$
255	1.2×10^{-3}	90	1.6×10^{-3}	90	$(1.4 \pm 0.2) \times 10^{-3}$
265	7.6×10^{-4}	120	6.9×10^{-4}	210	$(7.3 \pm 0.3) \times 10^{-4}$
275	1.9×10^{-4}	240	1.2×10^{-4}	210	$(1.6 \pm 0.3) \times 10^{-4}$
285	2.4×10^{-5}	180	1.2×10^{-4}	270	$(7.2 \pm 4.8) \times 10^{-5}$

10. References

M. W. Powner, B. Gerland, J. D. Sutherland, *Nature*, 2009, **459**, 239-242.
S. Ranjan and D. D. Sasselov, *Astrobiology,* 2017, **17**, 169-204.
S. Rugheimer, A. Segura, L. Kaltenegger, D. Sasselov, *Astrophys. J.,* 2015, **806**, 137-147.